Mechanism of the Vinylcyclopropane−Cyclopentene Rearrangement Studied by Quasiclassical Direct Dynamics

Charles Doubleday*

Department of Chemistry, Columbia University, New York, New York 10027

Received: February 7, 2001; In Final Form: April 23, 2001

The stereochemical course of the thermal rearrangement of vinylcyclopropane to cyclopentene is computed using quasiclassical trajectories run on a modified AM1 potential parametrized to fit ab initio calculations. At 573 K, 34000 trajectories are initialized quasiclassically with a Boltzmann distribution at 3 transition state (TS) structures, trideuterated for a total of 8 diastereomeric TSs. The computed product ratio is *si*:*sr*:*ar*:*ai* = 42:30:10:18 (exptl 40:23:13:24), where *s*,*a* refers to suprafacial or antarafacial allylic participation and *r*,*i* refers to retention or inversion of the migrating methylene. Initialization at each TS leads to all 4 products—that is, the product distribution is entirely under dynamical control. The temperature dependence of the product ratio over 400−1000 K is small. At 573 K, 83% of the trajectories have lifetimes under 400 fs. For times $t < 400$ fs the product ratio is strongly time-dependent; for $t > 400$ fs the product ratio is approximately constant and closer to statistical. However, trajectories initialized at the 3 TS structures do not give identical product distributions under any circumstances. Root-mean-square angular velocities of the torsions are approximately constant over nearly the entire course of the reaction. These data demonstrate nonstatistical dynamics and are inconsistent with a mechanism involving a statistical intermediate. Instead, the mechanism consists of 4 competing direct reactions.

1. Introduction

We present a computational study of the vinylcyclopropane (VCP) rearrangement to cyclopentene (CP), the simplest 1,3 sigmatropic carbon shift.[1,2] Its archetypal status has made it an important testing ground for the degree of stereochemical control exerted by the Woodward−Hoffmann rules and for the existence of intermediates in thermal isomerizations. The VCP rearrangement typically produces both W-H allowed and forbidden products. With most substituents[1,2] there is a mild (in some cases, strong[3]) preference for W-H allowed reaction. Baldwin and Anet[4] reported the pyrolysis of the triply deuterated parent compounds *syn*-*E*- and *syn*-*Z*-VCP-d_3 at 573 K. The product distribution (Figure 1) is *si*:*sr*:*ar*:*ai* = 40:23:13:24, where *s* and *a* refer to suprafacial or antarafacial allylic participation and *r* and *i* refer to retention or inversion of the migrating methylene. The ratio of allowed (*si* + *ar*) to forbidden (*sr* + *ai*) products is ∼1:1, consistent with a biradical intermediate or with a set of competing direct reactions.

Recently Houk and co-workers[5] and Davidson and Gajewski[6] examined this reaction with complementary electronic structure methods. Houk used DFT with 4-electron-4-orbital complete active space MCSCF (4,4-CAS) energy corrections, 4,4-CAS/6-31G*//(U)B3LYP/6-31G*, and Davidson and Gajewski optimized stationary points with 4,4-CAS/6-31G*. The calculations agree on several points. There is no well-defined local minimum in the biradical region of the potential energy surface (PES).[7] Instead, there is a broad flat region where all 4 paths are within 2−3 kcal/mol of each other. The lowest energy transition state (TS) capable of mediating the 1,3-shift is TS13 (Figure 2), whose intrinsic reaction coordinate[8] (IRC) corresponds to *si*. In fact, this is the only TS whose IRC involves a 1,3-shift. To account for the other 3 paths, both groups point out that the PES is flat enough to allow two or more paths to merge at TS(90,0) and TS(0,0). Qualitatively, this accounts for all 4

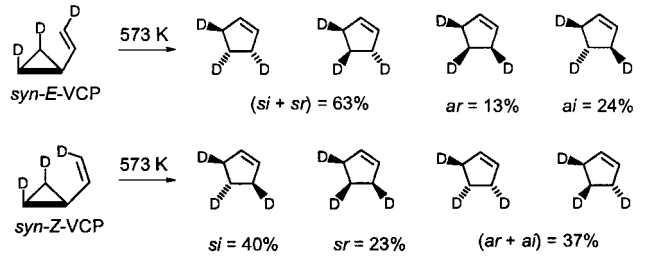

Figure 1. Experimental results of Baldwin and Anet (ref 4), where *s*,*a* refers to suprafacial or antarafacial allylic participation and *r*,*i* refers to retention or inversion of the migrating methylene.

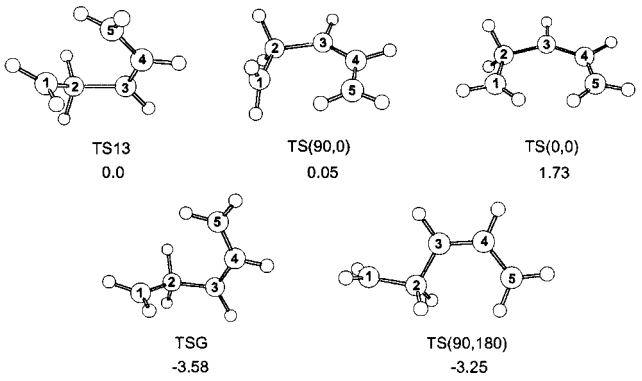

Figure 2. Saddle points on the AM1-SRP surface. TS(0,0), TS(90,0), and TS(90,180) have C_s symmetry; (*n*,*m*) denotes torsion angles about C_1-C_2 and C_2-C_3, respectively. AM1-SRP relative energies (kcal/mol) are from ref 18. The IRC passing through TS13 corresponds to the 1,3 shift. IRCs passing through the other four involve VCP stereoisomerization.

* E-mail: ced3@columbia.edu.

10.1021/jp010464z CCC: $20.00
Published on Web 06/05/2001

reactions. However, if a single TS mediates two or more reaction paths, then transition state theory (TST) as currently applied[9] cannot predict a unique product ratio without additional dynamical assumptions.[10]

For this reason we have resorted to quasiclassical trajectories, in which the product ratio is given simply by a trajectory count. We employ direct dynamics, in which the classical nuclear motion (dynamics) is computed directly from AM1[11] electronic structure calculations, suitably modified and reparametrized. ("Direct dynamics" has been in use for a number of years[12] to denote variational TST calculations[9] in which partition functions are computed directly from electronic structure theory, a calculation that bypasses the nuclear dynamics to yield rate constants.) Our goal is to compute the *si:sr:ar:ai* ratio and describe the mechanism. Among the important mechanistic questions are whether the reaction involves an intermediate, and whether the dynamics is statistical or nonstatistical. Recent trajectory studies of trimethylene,[13,14] and prior trajectory studies of 1,3-shifts and other reactions by Carpenter,[10,15] have yielded a better appreciation of the role of nonstatistical dynamics in stereoselection.

The conundrum one encounters in using TST to interpret the VCP rearrangement was discussed many years ago by Doering,[16] who proposed a "continuous diradical" model for the transition state. The model involves dynamically continuous ring opening to a flat plateau on the PES, internal rotation, and cyclization, without a barrier-protected intermediate. Doering proposed that instead of a single mechanism we embrace a family of mechanisms, all operating within the plateau region. His model emphasizes the difficulty (by implication the futility) of trying to distinguish between TSs that share the same region of phase space. Baldwin[17] has recently proposed a model for the VCP rearrangement in which substantial stereochemical scrambling occurs (without an intermediate) in regions of the PES below the TS energy. This model implies that the TS below which these stereochemical paths diverge cannot be used to predict the partitioning between them. A related issue is nonstatistical dynamics. A number of years ago, Carpenter[15] proposed that torsional motions, which govern stereochemistry, tend to conserve angular momentum as the trajectory moves through the TS region of 1,3-shifts and certain other isomerizations. This conflicts with RRKM theory, which requires that intramolecular vibrational redistribution (IVR) be much faster than chemical reaction. If IVR were globally fast, then torsional motion could not continue very far without its energy being diverted into other modes. In Carpenter's model, energy transfer between torsional and nontorsional modes is slower than the reciprocal lifetime of the trajectory. This model has received strong support from trajectory studies on model and semiempirical PESs,[15] and more recently on realistic PESs for trimethylene[13,14] and in a preliminary version of the present work.[18]

In this calculation we examine the dynamics of isomerization of *syn-E*-VCP as the formal reactant, and assume that exclusion of *syn-Z*-VCP will not affect the results significantly. Although deuterium labeling is necessary to reveal the stereochemistry experimentally (for which both *syn-E*- and *syn-Z*-VCP are required), calculations do not require it because each atom is unique. However, we adhere to Baldwin's deuteration pattern because the dynamics of internal rotation depends on the atomic masses.

2. AM1-SRP Potential Energy Surface

The ab initio PES is fitted by AM1 with specific reaction parameters (AM1-SRP). The BIRADICAL keyword in MOPAC is used to invoke the half-electron method[19] with 3 × 3 CI involving two electrons occupying HOMO and LUMO. A Levenberg−Marquardt nonlinear least squares program is used to minimize the sum of squares,

$$w_E{}^2 \sum_i (E_i - E_i{}^0)^2 + w_R{}^2 \sum_i (R_i - R_i{}^0)^2 + w_A{}^2 \sum_i (A_i - A_i{}^0)^2 + w_D{}^2 \sum_i (D_i - D_i{}^0)^2$$

where the difference terms involve AM1-SRP minus ab initio values of energies E_i (MRCI/cc-pVDZ energies[18] of the structures in Figure 2, experimental $\Delta H^{\ddagger}$,[20] relative energy of VCP and CP), C−C bond lengths R_i, C−C−C bond angles A_i, and selected dihedral angles D_i of the geometries in Figure 2, which shows the AM1-SRP saddle points. The weights are $w_E = 1.0$ mol/kcal, $w_R = 5.0$ Å^{-1}, $w_A = 0.08$ degree^{-1}, $w_D = 0.05$ degree^{-1}.

The fit includes 12 AM1 parameters for C and 5 for H. Resonance integrals, core−core repulsions, and electron−nuclear attraction terms are multiplied by constant scaling factors χ_{ij} for $ij = C_1C_2$, C_2C_3, C_3C_4, C_4C_5, and a single χ value for all C−H pairs. Resonance integrals for $ij = C_1C_3$ and C_1C_5 are multiplied by distance-dependent functions $\chi(R_{ij})$ containing a tanh function that switches smoothly between values of $\chi(R_{ij})$ appropriate for large and small ij distance R_{ij}. Analytical terms are added to correct the otherwise small allylic internal rotation barriers. AM1-SRP is fully defined in the Supporting Information of this paper. Energies, geometries, and frequencies of stationary points in Figure 2 are also listed in the Supporting Information. The AM1-SRP relative energies of the saddle points in Figure 2 have an average absolute deviation of 0.2 kcal/mol from the relative ab initio energies reported by Houk and co-workers[5] and Davidson and Gajewski.[6] These energies were reported in our preliminary communication[18] and are included in the current Supporting Information. The saddle point geometries are close to ab initio geometries,[21] frequencies are reasonably close, transition vectors are similar, and the IRC passing through TS13 is similar to that reported by Houk and co-workers.[5]

Figure 3 shows selected points along the IRC that passes through TS13. It is very asymmetric, with a steep drop on the CP side and a large flat region on the VCP side. All the stereochemical lability lies in the flat region. Once a trajectory passes through TS13 on its way to CP, the stereochemistry present at TS13 is captured and preserved in a specific CP isomer.

3. Procedures for the Trajectory Simulations

In this study we simulate the dynamics of the VCP rearrangement in the high-pressure limit, corresponding to a Boltzmann distribution of reactant energy levels. Our approach is to focus on the dynamics of the biradicaloid TS region of the PES. We assume that intramolecular vibrational energy redistribution (IVR) is fast in VCP, so that a microcanonical ensemble of reacting molecules is maintained at each energy.[22] This implies a canonical Boltzmann distribution of reacting molecules in the high pressure thermolysis of VCP. We further assume that a Boltzmann distribution applies to the transition states. This suggests the following procedure: initialize a set of trajectories at each TS that can be reached from the reactant *syn-E*-VCP following initial C_1-C_3 bond cleavage, and average the results with weights proportional to the partition function at each TS. Figure 4 lists the 8 trideuterated TS structures that

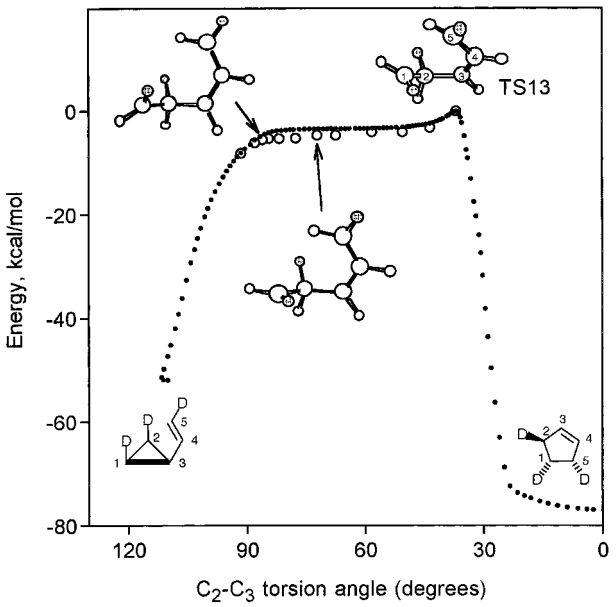

Figure 3. Selected points along the IRC passing through TS13, leading to *si* reaction. Dots are AM1-SRP energies, uncorrected by ZPE. Circles are free energies at 573 K.

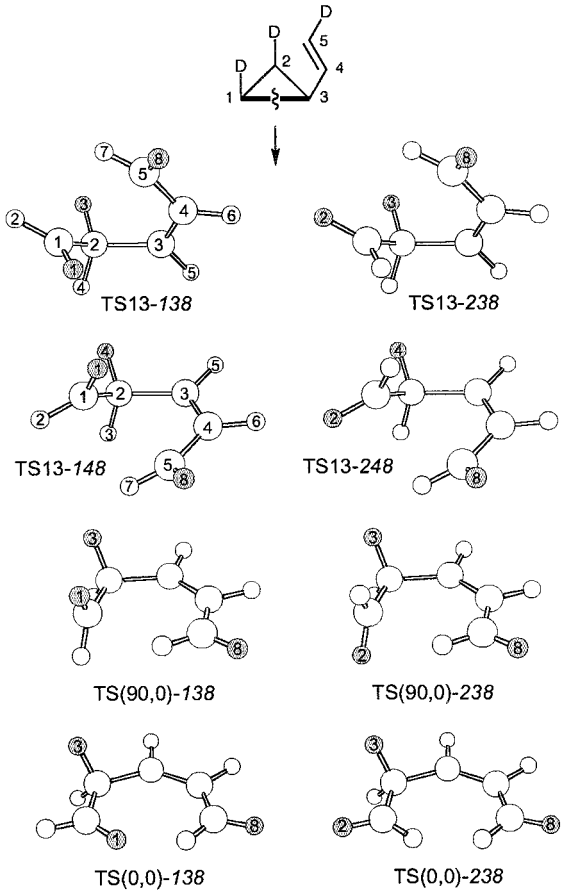

Figure 4. Eight diastereomeric TS structures reachable by C_1-C_3 cleavage of *syn-E*-VCP. Numbers at the end of the name indicate deuterium positions (shaded). The numbering in TS13-*148* and TS13-*248* reflects their mirror-image structural relationship to TS13-*138* and TS13-*238*.

can be reached from *syn-E*-VCP following initial C_1-C_3 bond cleavage. We ignore the enantiomeric set of 8 structures formed by C_2-C_3 bond cleavage. The flatness of the PES[5,6,18] guarantees that the rotations about C_1-C_2 and C_2-C_3 necessary to reach all these structures from *syn-E*-VCP can be accomplished at energies below the TS energies.

The semiempirical direct dynamics trajectories reported here were calculated with VENUS-MOPAC,[23] a combination of the dynamics program VENUS 96[24] with the MOPAC 7 semiempirical electronic structure package.[25] To compute the trajectories we incorporated AM1-SRP into a parallel version of VENUS-MOPAC, run on the SGI Origin 2000 at the National Center for Supercomputer Applications.

A. Sampling of Initial Conditions. The TS normal mode sampling procedure[26] is used to generate a set of initial coordinates and momenta that approximates a quantum mechanical Boltzmann distribution on a TS dividing surface. In this procedure, the initial coordinates and momenta are based on harmonic vibrational energy levels computed from the Cartesian second derivative matrix. The sampling is carried out quasiclassically,[27] which means that each vibrational normal mode receives at least the zero point energy, and any additional energy is added in discrete quanta so that the initial energy distribution for each vibrational mode is in accord with quantum mechanics. After the trajectory begins, this condition is relaxed and the system evolves according to classical mechanics. The choice of the number of vibrational quanta for each normal mode, the vibrational amplitude, momentum, and phase of each mode, the momentum and phase of the reaction coordinate, and the sampling of a Boltzmann distribution of angular momentum have all been described in detail for application to trimethylene dynamics.[26]

B. Trajectory Integration. After initial conditions are selected, Hamilton's equations of motion are integrated in Cartesian coordinates and momenta with a combined 4th-order Runge-Kutta and 6th-order Adams-Moulton predictor−corrector algorithm.[28] Every trajectory is integrated forward and backward in time until a product (VCP or CP) is formed in each direction. When a forward-time segment ends, the backward-time segment begins, initialized with the original coordinates and momenta with which the forward segment was initialized, using negative time steps. At each step of the integration the Schroedinger equation is solved according to the AM1-SRP prescription. The first derivative of the energy with respect to Cartesian atomic positions is computed by the Dewar-Liotard[29] analytical CI method in MOPAC 7. The integration step size is 0.25 fs, and energy is conserved to 4−5 significant figures over a typical trajectory.

C. Final Trajectory Conditions; Methods for Counting Reactive Trajectories. The criterion for VCP formation is that $C_1C_2C_3 < 75°$, and the criterion for CP formation is that $C_1C_5 < 1.8$ Å. If either of these criteria is met, the trajectory segment (forward-time or backward-time) is stopped and the stereochemistry is recorded. A trajectory is unreactive if the forward-time and backward-time trajectory segments both give VCP or both give CP, in which case a 1,3-shift is not involved. The minimum requirement for a trajectory to be reactive is that it gives a 1,3-shift—that is, either the forward or backward trajectory segment leads to VCP and the other segment leads to CP.

We consider two methods for counting reactive trajectories. In method 1, we include all 1,3-shifts derived from trajectories initialized at a given TS with a given trideuteration pattern (trajectories were initialized at 8 such TS structures in all, see Figure 4). For example, Figure 5 shows four VCP−CP pairs linked by *si*, *sr*, *ar*, *ai* trajectories initiated at TS13-*138*. The stereochemistry of the reaction is determined by comparing VCP and CP stereoisomers at the termini of the forward-time and

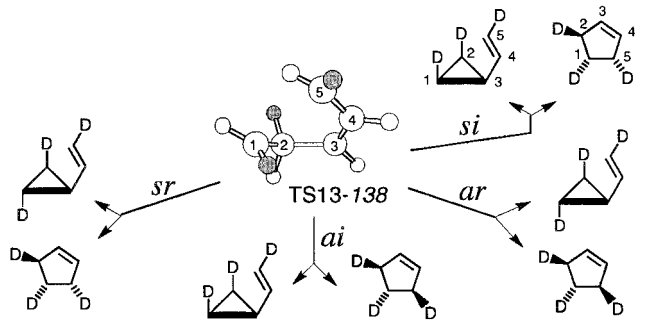

Figure 5. Representative pairs of VCP−CP structures connected via initialization at TS13-*138*, and included in the list of reactive trajectories counted by method 1 (see text). Additional VCP−CP pairs are also formed in which, for example, the vinyl group of VCP is trans to C_2-D. All these VCP−CP pairs are counted by method 1.

backward-time segments. Note that a variety of VCP stereoisomers may be formed by initialization at a given TS stereoisomer (TS13-*138* in this example), even though Baldwin's experiment involves only *syn-E*-VCP or *syn-Z*-VCP. Method 1 was used in our preliminary communication.[18]

In method 2, a trajectory is reactive if and only if the 1,3-shift involves formation of *syn-E*-VCP. 1,3-shifts in which any other VCP isomer is formed are considered unreactive. Method 2 allows us to construct an ensemble of trajectories initialized at the 8 TSs of Figure 4, which lead only to the VCP and CP isomers shown in the top half of Figure 1, and no others. This method corresponds more directly to experiment than method 1, which includes trajectories that produce various isomers of *syn-E*-VCP. The disadvantage of method 2 is that it gives a smaller percentage of reactive trajectories than method 1. In the absence of a stereochemical isotope effect on the dynamics, the two counting methods should give the same product distribution. However, we shall see that the trideuteration pattern of the TS can affect the product distribution.

4. Product Distribution Derived from Trajectories

We seek the product ratio F_{si}:F_{sr}:F_{ar}:F_{ai}, where F_ρ is the fractional yield of reaction ρ (*si*, *sr*, *ar*, *ai*), with $F_{si} + F_{sr} + F_{ar} + F_{ai} = 1$. For trajectories initialized at a particular TS θ (TS13, TS(90,0), TS(0,0)) with trideuteration pattern d (one of the 8 structures in Figure 4), let $F^d{}_{\theta,\rho}$ be the fractional yield of reaction ρ,

$$F^d_{\theta;\rho} = \frac{N^d_{\theta;\rho}}{N^d_\theta} \tag{1}$$

where $N^d{}_{\theta,\rho}$ is the number of trajectories that produce reaction ρ and $N^d{}_\theta = N^d{}_{\theta,si} + N^d{}_{\theta,sr} + N^d{}_{\theta,ar} + N^d{}_{\theta,ai}$ is the total number of reactive trajectories, counted by either of the two methods for counting reactive trajectories. F_ρ is computed from

$$F_\rho = A/W$$

$$A = W^{138}_{13} F^{138}_{13;\rho} + W^{148}_{13} F^{148}_{13;\rho} + W^{238}_{13} F^{238}_{13;\rho} + W^{248}_{13} F^{248}_{13;\rho} + W^{138}_{90,0} F^{138}_{90;0;\rho} + W^{238}_{90,0} F^{238}_{90,0;\rho} + W^{138}_{0,0} F^{138}_{0,0;\rho} + W^{238}_{0,0} F^{238}_{0,0;\rho}$$

$$W = W^{138}_{13} + W^{148}_{13} + W^{238}_{13} + W^{248}_{13} + W^{138}_{90,0} + W^{238}_{90,0} + W^{138}_{0;0} + W^{238}_{0,0} \tag{2}$$

where $W^d{}_\theta$ is the weight applied to $F^d{}_{\theta,\rho}$ in the average, given by

$$W^d_{13} = R^d_{13}\, Q^d_{13} e^{-E^d_{13}/k_B T}, \quad d = 138, 148, 238, 248 \tag{3a}$$

$$W^d_{90,0} = R^d_{90,0}\, Q^d_{90,0} e^{-E^d_{90,0}/k_B T}, \quad d = 138, 238 \tag{3b}$$

$$W^d_{0,0} = R^d_{0,0}\, Q^d_{0,0} e^{-E^d_{0,0}/k_B T}, \quad d = 138, 238 \tag{3c}$$

Here, $R^d{}_\theta$ is the reactive fraction of trajectories initialized at TS θ with trideuteration pattern d, computed by one of the two counting methods. $Q^d{}_\theta$ is the product of the vibrational and classical rotational partition function for TS θ with trideuteration pattern d, $E^d{}_\theta$ is the ZPE-corrected energy, k_B is the Boltzmann constant, and T is the temperature. $Q^d{}_\theta$ is given by

$$Q^d_\theta = Q^{rot}_{class}\, Q^{vib}_{harm}\, Q^{vib,i}_{hr} / Q^{vib,i}_{harm} \tag{4}$$

where (with suppression of d, θ super/subscripts on the right side) $Q^{rot}{}_{class}$ is the classical rotational partition function, $Q^{vib}{}_{harm}$ is the harmonic partition function for the 32 bound vibrational modes orthogonal to the transition vector, $Q^{vib,i}{}_{harm}$ is the harmonic partition function for the single vibrational mode i assigned to an internal rotation, and $Q^{vib,i}{}_{hr}$ is the hindered rotor partition function for mode i. The transition vector of each TS is assigned to internal rotation about C_1-C_2 or C_2-C_3. Therefore, the other internal rotation, mode i, is one of the 32 bound modes. Its harmonic partition function, $Q^{vib,i}{}_{harm}$, is replaced by $Q^{vib,i}{}_{hr}$ in eq 4. $Q^{vib,i}{}_{hr}$ is computed by the method of Pitzer and Gwinn,[30] which requires the internal rotation barrier and reduced moment of inertia. AM1-SRP barriers are computed by constrained minimizations at a series of torsion angles, optimizing only bond lengths and bond angles and fixing all dihedral angles. The barriers are 3.19 kcal/mol for C_1-C_2 rotation in TS13, 2.24 kcal/mol for C_1-C_2 rotation in TS(90,0), and <0.1 kcal/mol for C_2-C_3 rotation in TS(0,0). The ratio $Q^{vib,i}{}_{hr}/Q^{vib,i}{}_{harm}$ in eq 4 is 2.72, 2.42, 4.87 for TS13, TS(90,0), TS(0,0), respectively, and is insensitive to the trideuteration pattern.

5. Statistical Theory

TST does not give a unique prediction of the product ratio, because all four reactions are accessible from TS13, TS(90,0), and TS(0,0). TST, whether conventional or variational, accounts for the total reactive flux through a given TS, but gives no guidance about the partitioning among four reactions whose paths diverge below the TS energy.

We find no free energy minimum along the IRC passing through TS13 using canonical VTST[9b] with harmonic partition functions. The open circles in Figure 3 show the free energy change through the flat region of the IRC. At 573 K, the decrease in entropy along the path is small until the cyclopropane ring starts to form, at which point the steep decrease in energy overwhelms the smaller rise in $-T\Delta S$.

6. Trajectory Results and Discussion

A. 573 K. Table 1 lists the partition functions, reactive fractions, and other quantities used in eqs 3 and 4. Tables 2 and 3 show the stereochemical product distributions obtained from initialization at the 8 trideuterated TSs of Figure 4 at 573 K, using the two counting methods. The standard deviation $\sigma^d{}_{\theta,\rho}$ (ρ = *si*, *sr*, *ar*, *ai*) for initialization at TS θ with deuteration pattern d is estimated from the binomial distribution using[31] $\sigma^d{}_{\theta,\rho} = [F^d{}_{\theta,\rho}(1 - F^d{}_{\theta,\rho})/N^d{}_\theta]^{1/2}$, where $F^d{}_{\theta,\rho}$ and $N^d{}_\theta$ are given in eq 1. Table 4 shows the final product distribution computed from eq 2 using the two counting methods, with comparison to experiment.

TABLE 1: Boltzmann Factors, Partition Functions, Reactive Fractions, and Relative Weights Used in Eqs 3, 4

			counting method 1		counting method 2	
TS	$e^{-\Delta E^d_\theta/k_BT}$	$Q^d_\theta/10^9$	reactive fraction R^d_θ	rel. wt. W^d_θ	reactive fraction R^d_θ	rel. wt. W^d_θ
TS13-*138*	1	0.124	0.867	1	0.399	1
TS13-*148*	1	0.124	0.888	1.02	0.086	0.216
TS13-*238*	0.98	0.124	0.879	0.99	0.350	0.860
TS13-*248*	0.98	0.124	0.887	1.00	0.092	0.226
TS(90,0)-*138*	0.93	0.218	0.180	0.339	0.056	0.229
TS(90,0)-*238*	0.93	0.219	0.174	0.330	0.055	0.226
TS(0,0)-*138*	0.21	0.999	0.146	0.289	0.019	0.082
TS(0,0)-*238*	0.21	1.11	0.127	0.279	0.050	0.239

Trajectories initialized at TS13 dominate the results, because they have much higher reactive fractions (R^d_θ in eq 3) than trajectories initialized at TS(90,0) or TS(0,0). This result is expected from the IRCs. TS13 is the only saddle point whose IRC connects VCP with CP. IRCs of the other two TSs lead to cis−trans isomerization of VCP via the broad flat region of the PES.

Tables 2 and 3 appear different, but both counting methods predict similar product ratios in Table 4, which agree reasonably well with experiment. The most obvious difference between Tables 2 and 3 is the apparent stereospecificity of trajectories initialized at TS13 in Table 3. This is a consequence of counting method 2, which includes only the trajectories that form *syn-E*-VCP. As trajectories pass through TS13 going toward CP, the steep drop in energy (Figure 3) captures the stereochemistry present at TS13 and preserves it in a single CP isomer. Thus *syn-E*-VCP is connected via TS13 to nearly 100% of a single CP isomer in Table 4. A stereochemical isotope effect in which the d_3 pattern affects the product ratios can be seen in TS(0,0)-*138* vs TS(0,0)-*238* in Table 3 and in TS13-*148* vs TS13-*238* in Table 2. Since isotopomers evidently have somewhat different dynamical properties, counting method 1 (which counts trajectories leading to several VCP isotopomers) suffers from the implicit assumption that this stereochemical isotope effect is absent. Method 2, in contast, imposes fewer dynamical assumptions because it counts only trajectories leading to *syn-E*-VCP, the molecule actually used in Baldwin's experiment. Therefore, we shall adopt the product ratios derived from method 2 as the predicted ratios. The agreement between theory and experiment in Table 4 gives us a degree of confidence that dynamical information derived from the trajectories will be useful for describing the mechanism of the isomerization.

Tables 2 and 3 suggest the VCP rearrangement does not occur in two steps via a statistical intermediate, because the product ratios derived from TS13, TS(90,0), and TS(0,0) are different. If the reaction did proceed via a statistical intermediate, then trajectories starting at the 3 TSs would be expected to give the same product ratio as a result of fast IVR to form a common intermediate.

Figure 6 shows the survival probability $S(t)$ for reactive trajectories at 573 K counted by method 2, averaged over the 8 TS structures accessible to *syn-E*-VCP (Figure 4). $S(t)$ is computed from

$$S(t) = B/W$$

$$B = W^{138}_{13}\,S^{138}_{13}(t) + W^{148}_{13}S^{148}_{13}(t) + W^{238}_{13}\,S^{238}_{13}(t) + W^{248}_{13}\,S^{248}_{13}(t) + W^{138}_{90,0}\,S^{138}_{90,0}(t) + W^{238}_{90,0}S^{238}_{90,0}(t) + W^{138}_{0,0}\,S^{138}_{0,0}(t) + W^{238}_{0,0}\,S^{238}_{0,0}(t)$$

$$S^d_\theta(t) = N^d_\theta(t)/N^d_\theta(0) \qquad (5)$$

where W is the sum of weights W^d_θ (eqs 2, 3), $S^d_\theta(t)$ and $N^d_\theta(t)$ are, respectively, the survival probability at time t and the number of reactive trajectories of all stereochemistries that are still active at time t, for trajectories initialized at TS θ with trideuteration pattern d. After an initial period, the decay is approximately exponential from 300 to 1000 fs with a time constant τ of 220 fs. $S(t)$ decays to 0.5 in 230 fs. The initial 100 fs period with no decay is the minimum time necessary to cross the TS region of the PES, from VCP to CP. The reaction coordinate involves C_2-C_3 torsion and also C_1-C_2 torsion if inversion is involved. Figures S2 and S3 in the Supporting Information show a typical *si* and *ai* trajectory initialized at TS13-*138* and projected onto the C_1-C_2 and C_2-C_3 torsional space at 2.5 fs intervals.

TABLE 2: Percent Yields ± 2 Standard Deviations, from Trajectories Initialized at the 8 TSs of Figure 4, Counted by Method 1

	TS13				TS(90,0)		TS(0,0)	
	138	148	238	248	138	238	138	238
si	45.9 ± 2.8	48.6 ± 2.8	37.7 ± 2.7	41.1 ± 2.9	26.3 ± 2.4	27.5 ± 2.7	25.8 ± 2.6	31.0 ± 3.2
sr	34.0 ± 2.6	31.1 ± 2.6	39.4 ± 2.7	35.8 ± 2.8	26.9 ± 2.5	26.5 ± 2.6	17.6 ± 2.2	14.2 ± 2.4
ar	8.5 ± 1.5	10.0 ± 1.7	12.5 ± 1.8	12.7 ± 2.0	18.4 ± 2.1	17.1 ± 2.3	17.1 ± 2.2	13.4 ± 2.3
ai	11.5 ± 1.8	10.4 ± 1.7	10.4 ± 1.7	10.3 ± 1.8	28.4 ± 2.5	28.9 ± 2.7	39.5 ± 2.9	41.4 ± 3.4
no. traj.[a]	1512	1436	1450	1286	7287	6382	7866	6754
% reac.[b]	86.7	88.8	87.9	88.7	18.0	17.4	14.6	12.7

[a] Total number of trajectories. [b] Percent of trajectories that are reactive.

TABLE 3: Percent Yields ± 2 Standard Deviations[a] from Trajectories Initialized at the 8 TSs of Figure 4, Counted by Method 2

	TS13				TS(90,0)		TS(0,0)	
	138	148	238	248	138	238	138	238
si	99.4 ± 0.7	0 ± 3	1.6 ± 1.2	0.9 ± 2.3	42.2 ± 4.9	42.2 ± 5.3	20.4 ± 6.8	32.5 ± 5.1
sr	0.2 ± 0.9	1 ± 4	97.6 ± 1.4	0.9 ± 2.3	5.1 ± 2.3	5.7 ± 2.6	30.6 ± 7.7	11.9 ± 3.6
ar	0.2 ± 0.9	99 ± 2.2	0.6 ± 0.8	0.9 ± 2.3	5.1 ± 2.3	3.7 ± 2.2	30.6 ± 7.7	11.0 ± 3.5
ai	0.2 ± 0.9	0 ± 3	0.2 ± 0.5	97.3 ± 3.4	47.5 ± 5.0	48.3 ± 5.4	18.4 ± 6.6	44.5 ± 5.5
no. traj.[b]	1512	1436	1450	1286	7287	6382	7866	6754
% reac.[c]	39.9	8.6	35.0	9.2	5.6	5.5	1.9	5.0

[a] For percentages near 0 or 100, the 95% confidence interval is computed from the exact binomial distribution using the calculator at http://members.aol.com/johnp71/confint.html#Binomial. In such cases, the confidence interval is written as ±x, where x is the larger of the two exact confidence limits. [b] Total number of trajectories. [c] Percent of trajectories that are reactive.

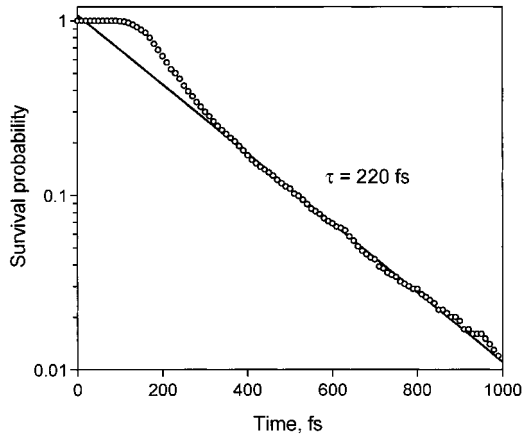

Figure 6. Survival probability $S(t)$, eq 5, for reactive trajectories at 573 K counted by method 2, averaged over the 8 TS structures of Figure 4. The time constant τ is determined by a fit from 300 to 900 fs (straight line).

TABLE 4: Percent Yields Computed from Eq 2, ± 2 Standard Deviations

	method 1[a]	method 2[b]	expt.[c]
si	39.6 ± 1.2	42.1 ± 0.8	40
sr	31.9 ± 1.1	30.0 ± 0.9	23
ar	12.3 ± 0.5	9.6 ± 0.6	13
ai	16.2 ± 0.6	18.3 ± 0.8	24

[a] Counting all [1,3] shifts. [b] Counting only [1,3] shifts involving *syn*-[*E*-VCP. [c] ±2−3% (ref 4).

TABLE 5: Time-Dependent Product Yields, Counted by Method 2, Averaged According to Eq 2

	percent yields[a]				ratios[b]	
range, fs	*si*	*sr*	*ar*	*ai*	*s/a*	*i/r*
0−100	0	0	0	0		
100−200	16.1	13.3	0.0	1.2	23.7	1.3
200−300	15.1	7.3	0.8	6.0	3.3	2.6
300−400	4.7	4.1	2.1	3.5	1.6	1.3
400−500	2.4	1.8	2.5	2.3	0.9	1.1
500−600	1.3	1.3	1.8	2.2	0.6	1.1
600−700	0.8	1.0	1.0	0.9	0.9	0.9
700−800	0.4	0.3	0.8	0.8	0.5	1.1

[a] The yields sum to 95.8%, the amount formed in 800 fs. [b] $s/a = (si + sr)/(ai + ar)$; $i/r = (si + ai)/(sr + ar)$.

Table 5 shows the time development of the products at 100 fs intervals averaged over all 8 TSs according to eq 2. Time-dependent product ratios are a clear indication of nonstatistical dynamics, because a Boltzmann distribution of energy levels must give a single product distribution that depends only on the temperature. The trajectories are initialized with a Boltzmann distribution, but deviate from that condition by the time products are formed. The time scale for product formation is short (Figure 6), because the trajectories cyclize whenever the termini approach with the right orientation. This evidently reduces the trajectory lifetimes well below the time required for IVR.

Table 6 shows the contributions to *a/s* and *i/r* ratios from each of the 3 TSs, separately averaged over the trideuteration patterns using the weights $W^d{}_\theta$ in eq 3. The strong time dependence of *s/a* in Table 5 is dominated by trajectories initialized at TS13. This is because *s* and *a* trajectories reach TS13 by different routes. Of the trajectories initialized at TS13, 81% of *a* trajectories proceed by way of an anti biradical conformation (C_2-C_3 torsion angle of 180°), whereas only 3% of *s* trajectories do.[32] This is illustrated in Figure 7. After C_1-C_3 bond cleavage, *s* reaction occurs mainly by least motion

TABLE 6: Time-Dependent Product Ratios[a] Derived from 3 TSs,[b] Counted by Method 2

	TS13		TS(90,0)		TS(0,0)	
range, fs[c]	*s/a*	*i/r*	*s/a*	*i/r*	*s/a*	*i/r*
100−200	463	1.2	0.5	88	1.3	7.1
200−300	11	1.7	0.8	23	0.5	9.9
300−400	2.3	0.8	1.0	9.8	0.9	1.7
400−500	0.7	0.8	1.5	9.1	1.3	0.7
500−600	0.6	0.8	0.7	10.7	1.2	1.3
600−700	0.6	0.6	1.8	2.8	1.2	0.6
700−800	0.2	0.7	0.9	2.3	0.9	1.3

[a] $s/a = (si + sr)/(ai + ar)$; $i/r = (si + ai)/(sr + ar)$. [b] Averaged over the isotopomers of each TS in the manner of eq 2. TS13 ratios are derived from product yields averaged over TS13-*138*, TS13-*238*, TS13-*148*, TS13-*248*; TS(90,0) and TS(0,0) are each averaged over d_3 patterns *138*, *238*. [c] No products are formed in <100 fs.

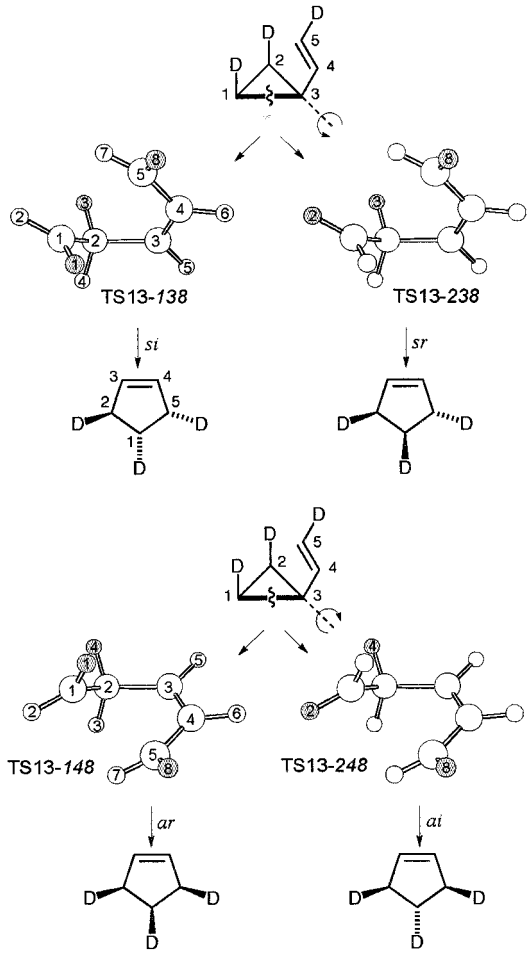

Figure 7. Main paths of trajectories leading from *syn-E*-VCP to CP via TS13. Suprafacial reaction occurs mainly by least-motion counterclockwise rotation of the vinyl group about C_2-C_3. Antarafacial reaction occurs mainly by nonleast-motion clockwise C_2-C_3 rotation of the vinyl group through an anti conformation before passing through TS13.

counterclockwise rotation of the vinyl group about C_2-C_3, passing through TS13 on the way to CP. Most of the *a* reaction occurs by clockwise C_2-C_3 rotation of the vinyl group through an anti conformation (C_2-C_3 torsion angle of 180°, e.g., TS-(90,180)), continuing on to TS13-*148* or TS13-*248*, then on to form CP. The C_2-C_3 torsional motion of these *a* trajectories involves a much greater angular distance of travel from *syn-E*-VCP to CP than *s* trajectories. Therefore *a* trajectories take a longer time. High cyclization efficiency implies that *s/a* is kinetically determined by the relative times of travel along the

s and *a* paths, and that *s/a* should be time-dependent. The *i/r* ratio also shows a strong time dependence in trajectories initialized at TS(90,0), whose transition vector is the C_1-C_2 torsion which determines *i* vs *r*.

Trajectories with lifetimes longer than 400 fs (83% decay of $S(t)$) have different dynamical properties from short-lived trajectories (lifetimes < 300 fs). Carpenter, in a trajectory study of a 1,3 sigmatropic shift,[15c] has suggested that the nonstatistical dynamical component is confined to short times and long-lived trajectories behave statistically. Tables 5 and 6 document the nonstatistical component at short times, and also reveal a species with different dynamical character at long times. The degree to which the long-lived trajectories behave statistically cannot be computed exactly, but we have three qualitative expectations of a statistical intermediate. The first is a large amount of stereorandomness. Second, the product ratio should not change with time. Third, product formation must be slower than IVR, so that product ratios should be the same for initialization at TS13, TS(90,0), and TS(0,0). In Table 5, and for a given TS in Table 6, the product ratios at $t > 400$ fs are roughly constant and for the most part in the vicinity of 1, the stereorandom value. However, the long time product ratio, especially *i*/*r*, is different for initialization at different TS structures. The dynamics at $t > 400$ fs is more statistical than at early times, but not fully statistical.

In summary, Tables 5 and 6 show a clear difference between short-lived trajectories (lifetimes < 300 fs) and long-lived trajectories (lifetimes > 400 fs), and neither exhibits fully statistical dynamics. Short-lived trajectories are stereoselective and the product ratio is strongly time dependent. Long-lived trajectories, most of which proceed via an anti conformation,[32] are much more stereorandom and their product ratios are relatively constant. However, long-lived trajectories are not fully stereorandom, and trajectories initialized at different TS structures give distinguishable product ratios even at long times.

Our finding of nonstatistical dynamics appears to be at odds with the assumption of Boltzmann equilibrium used to initialize the trajectories. This situation is unavoidable, because initialization at a saddle point is a practical necessity in order to generate a usable fraction of reactive trajectories, and anything other than a Boltzmann distribution would be arbitrary. In fact, we do not know the true distribution of TS energy levels. The choice of an initial Boltzmann distribution at the three TSs is partly vindicated by the reasonable agreement with experiment in Table 4.

To examine the torsional dynamics further, we compute the rms (root-mean-square) cumulative torsional displacement $\Delta_{ij}(t)$ at time *t*, counted by method 2 and averaged over all reactive trajectories, given by

$$\Delta_{ij}(t) = (C/C')^{1/2}$$

$$C = W_{13}^{138} D_{13;ij}^{138}(t) + W_{13}^{148} D_{13;ij}^{148}(t) + W_{13}^{238} D_{13;ij}^{238}(t) + W_{13}^{248} D_{13;ij}^{248}(t) + W_{90,0}^{138} D_{90,0;ij}^{138}(t) + W_{90,0}^{238} D_{90,0;ij}^{238}(t) + W_{0,0}^{138} D_{0,0;ij}^{138}(t) + W_{0,0}^{238} D_{0,0;ij}^{238}(t)$$

$$C' = W_{13}^{138} N_{13}^{138}(t) + W_{13}^{148} N_{13}^{148}(t) + W_{13}^{238} N_{13}^{238}(t) + W_{13}^{248} N_{13}^{248}(t) + W_{90,0}^{138} N_{90,0}^{138}(t) + W_{90,0}^{238} N_{90,0}^{238}(t) + W_{0,0}^{138} N_{0,0}^{138}(t) + W_{0,0}^{238} N_{0,0}^{238}(t)$$

$$D_{\theta;ij}^{d}(t) = \sum_{n=1}^{N_{\theta}^{d}(t)} (\phi_{\theta;ij;n}^{d}(t) - \phi_{\theta;ij;n}^{d}(0))^2 \qquad (6)$$

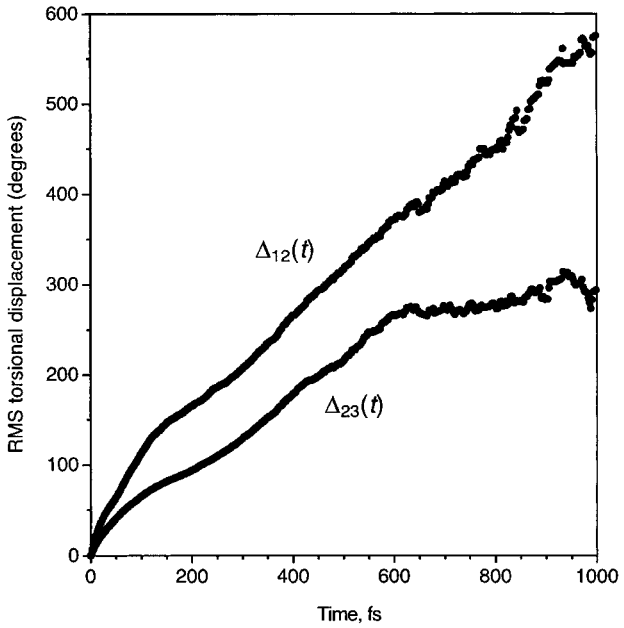

Figure 8. Root-mean-square cumulative torsional displacements, eq 6, counted by method 2 and averaged over all reactive trajectories.

where $\phi_{\theta,ij,n}^{d}(t)$ is the torsion angle about the *ij* bond (C_1C_2 or C_2C_3) in the *n*th trajectory at time *t*, initialized at TS θ with trideuteration pattern *d*. W_{θ}^{d} is given by eq 3, and $N_{\theta}^{d}(t)$ is given in eq 5. Each trajectory is reordered to start with VCP and end with CP. Thus $t = 0$ is the point at which VCP is formed in the original trajectory, all other points are at $t > 0$, and the final point is the formation of CP.

Plots of $\Delta_{12}(t)$ and $\Delta_{23}(t)$ (Figure 8) are remarkably close to linear over nearly the entire course of the reaction. $\Delta_{12}(t)$ is approximately linear over 100−1000 fs (99% decay of $S(t)$), and $\Delta_{23}(t)$ is approximately linear from 100 to 600 fs (93% decay of $S(t)$). The rms torsional angular velocities Ω are 8.7×10^{12} and 7.0×10^{12} rad s^{-1} for C_1-C_2 and C_2-C_3 torsion, respectively. The average time required for a 180° rotation is 360 fs for C_1-C_2 and 450 fs for C_2-C_3 torsion. A constant value of Ω is basically equivalent to Carpenter's nonstatistical model of torsional motion[15] in which torsional angular momentum is conserved.[33] It implies that the rms torsional kinetic energy ($I_r\Omega^2/2$, where I_r is the reduced moment of inertia) is constant and not being dissipated into other modes. The linear plots confirm that the trajectories are direct, that they move steadily, in an rms sense, from VCP to CP. Above 600 fs the change in slope of $\Delta_{23}(t)$ suggests that the longest-lived 7% of trajectories involves more complex, less direct C_2-C_3 torsional dynamics. At lifetimes this long, the change may be due in part to the well-known ZPE leakage effect,[34] an artifact of classical mechanics in which energy can flow between modes without the restriction of quantization.

B. Variable Temperature. In addition to 573 K, trajectories were initialized at TS13-*138* with quasiclassical TS normal mode sampling at 400, 500, 673, 800, and 1000 K to get a qualitative idea of the temperature dependence of the product distribution and trajectory lifetimes. The results are shown in Table 7. We used counting method 1 in order to maximize the number of trajectories available for analysis. No quantitative conclusions can be drawn from initialization at one TS isomer, but some qualitative features are evident. The time constants τ for decay of $S(t)$ are essentially constant over the 600 K range. The product distribution shows a weak temperature dependence in which *si* becomes more prominent at lower temperature. It was the absence of temperature dependence of the product ratio in a 1,3-shift that originally led Carpenter to propose that the product

TABLE 7: Temperature Dependence of Product Distribution from Trajectories Initialized at TS13-*138*, Counted by Method 1

	400 K	500 K	573 K	673 K	800 K	1000 K
no. traj.[a]	700	1430	1512	737	1000	1217
reac. frac.[b]	0.887	0.897	0.867	0.881	0.854	0.803
si	57.0 ± 4.0	49.6 ± 2.8	45.9 ± 2.8	47.3 ± 3.9	45.2 ± 3.4	40.3 ± 3.1
sr	24.5 ± 3.5	29.7 ± 2.6	34.0 ± 2.6	31.1 ± 3.6	30.6 ± 3.2	29.6 ± 2.9
ar	9.7 ± 2.4	9.1 ± 1.6	8.5 ± 1.5	7.9 ± 2.1	11.6 ± 2.2	14.6 ± 2.3
ai	8.9 ± 2.3	11.5 ± 1.8	11.5 ± 1.8	13.7 ± 2.7	12.6 ± 2.3	15.5 ± 2.3
τ[c]	192	202	223	198	209	197

[a] Total number of trajectories. [b] Fraction of trajectories that are reactive. [c] Time constant for decay of survival probability $S(t)$, fit over 250−800 fs. Uncertainty of τ is ca. ±10%.

ratio is under dynamical control.[15] The temperature dependence in Table 7 is not zero, but would be observable only over a large range. At high temperature, stereorandomness increases. At low temperature, *si* emerges as the dominant path. This is expected for trajectories initialized at TS13, because the minimum energy path between VCP and CP is the *si* IRC passing through TS13. Thus the temperature dependence appears to be due to the tendency of trajectories with less energy to follow the IRC. If this is true, one can speculate that the contribution to the temperature dependence from trajectories initialized at TS(90,0) and TS(0,0) should decrease at lower temperature, because the IRCs passing through TS(90,0) and TS(0,0) involve cis−trans isomerization of VCP, not the 1,3-shift. In the absence of these calculations, it does seem safe to conclude that the temperature dependence of the product distribution is very small over 400−1000 K.

Summary of the Mechanism

Quasiclassical trajectory calculations predict a mechanism consisting of 4 competing direct reactions. By direct, we mean that the reaction coordinate motion from reactant to product occurs rapidly and steadily, such that the reaction coordinate energy is not diverted to other modes and randomized (for example, in a local free energy minimum). For the VCP rearrangement, whose reaction coordinate involves internal rotation, direct reaction means that the rms torsional angular velocities are approximately constant. The evidence for direct reaction is the rapid formation of products in Tables 5 and 6, and the rms cumulative torsional displacements in Figure 8, which shows nearly constant rms rates of C_1-C_2 and C_2-C_3 rotation over most of the reaction. Though direct, the mechanism is not concerted in the traditional sense in which bond-breaking and bond-making occur in concert. On the other hand, there is no evidence that requires a statistical intermediate. The picture of the reaction is this: as the VCP ring opens, the C_1-C_2 and C_2-C_3 torsions begin their rotations, and they continue this motion until either C_1 and C_5 approach to form CP or C_1 and C_3 approach to form VCP. The very high efficiency of cyclization is the overriding limitation on trajectory lifetimes. This implies there is not enough time for torsional motion to participate in IVR before the reaction is over. Torsional motion is approximately decoupled from other modes and the torsional dynamics is nonstatistical.

About 80% of the reaction takes place in the first 400 fs. To form a product on this time scale, the initial conditions must send the trajectory on its way with very little wasted motion. C_1 and C_5 must approach expeditiously, and the orbital orientation must be favorable for cyclization. In this early-time window, the initial conditions (for example, cw vs ccw C_2-C_3 rotation in Figure 7) have a profound effect on the product distribution. At times longer than 400 fs, the remaining ∼20% of trajectories give a product distribution much closer to statistical. Is this due to redistribution of torsional energy into other modes? For most long-lived trajectories, we think the answer is no. First, the time-dependent product ratios are not fully statistical at long times, as would be expected if IVR were complete. Second, according to Figure 8 most long-lived trajectories (up to 600 fs for C_2-C_3 torsion, up to 1000 fs for C_1-C_2) are still moving along with the same rms torsional angular velocity as at earlier times. These are trajectories whose initial conditions are such that the C_1-C_5 distance has remained large at $t > 400$ fs, or for which cyclization did not occur because of unfavorable orbital orientation. The large majority of trajectories with lifetimes over 400 fs also proceed via an anti biradical conformation.[32] Without invoking globally complete IVR or ZPE leakage,[34] long-lived trajectories are expected to have a large dispersion in torsional angular velocities, phases, and signs of rotation (cw/ccw), as a result of having missed earlier cyclization opportunities and having lived much longer than average. The large dispersion in torsional dynamics implies a more stereorandom ensemble of products.

Acknowledgment. We thank the National Science Foundation for funding, and the National Center for Supercomputer Applications for a grant of computer time. We are also very grateful to Prof. William L. Hase for his encouragement and for helpful discussions.

Supporting Information Available: AM1-SRP definition and parameters; energies, internal coordinates, and vibrational frequencies for the structures in Figure 2; a table of trajectory results and three figures. This material is available free of charge via the Internet at http://pubs.acs.org.

References and Notes

(1) Gajewski, J. J. *Hydrocarbon Thermal Isomerizations*; Academic Press: New York, 1980; pp 81−87.

(2) Baldwin, J. E. In *The Chemistry of the Cyclopropyl Group*, Vol. 2; Rappoport, Z., Ed.; Wiley: London, 1995; pp 469−493.

(3) (a) Gajewski, J. J.; Olson, L. P. *J. Am. Chem. Soc.* **1991**, *113*, 7432−3. (b) Gajewski, J. J.; Olson, L. P.; Willcott, M. R., III. *Ibid.* **1996**, *118*, 299−306.

(4) Baldwin, J. E.; Villarica, K. A.; Freedberg, D. I.; Anet, F. A. L. *J. Am. Chem. Soc.* **1994**, *116*, 10845.

(5) (a) Houk, K. N.; Nendel, M.; Wiest, O.; Storer, J. W. *J. Am. Chem. Soc.* **1997**, *119*, 10545−10546. (b) Nendel, M.; Sperling, D.; Wiest, O.; Houk, K. N. *J. Org. Chem.* **2000**, *65*, 3259−3268.

(6) Davidson, E. R.; Gajewski, J. J. *J. Am. Chem. Soc.* **1997**, *119*, 10543.

(7) Nendel et al. (ref 5b) report a shallow biradical minimum with (U)-B3LYP/6-31G* that disappears at the (4,4)-CASSCF/6-31G* level with ZPE correction using DFT frequencies.

(8) Fukui, K. *J. Chem. Phys.* **1970**, *74*, 4161.

(9) (a) Truhlar, D. G.; Garrett, B. C.; Klippenstein, S. J. *J. Phys. Chem.* **1996**, *100*, 12771−12800. (b) Truhlar, D. G.; Isaacson, A. D.; Garrett, B. C. In *Theory of Chemical Reaction Dynamics*; Baer, M., Ed.; CRC Press: Boca Raton, 1985; Vol. 4, p 65. (c) Hase, W. L. *Acc. Chem. Res.* **1998**, *31*, 659; *Ibid.* **1983**, *16*, 258.

(10) Peterson, T. H.; Carpenter, B. K. *J. Am. Chem. Soc.* **1992**, *114*, 766.

(11) Dewar, M. J. S.; Zoebisch, E. G.; Healy, E. F.; Stewart, J. J. P. *J. Am. Chem. Soc.* **1985**, *107*, 3902.

(12) Baldridge, K. K.; Gordon, M. S.; Steckler, R.; Truhlar, D. G. *J. Phys. Chem.* **1989**, *93*, 5107−5119.

(13) (a) Doubleday, C.; Bolton, K.; Hase, W. L. *Ibid.* **1997**, *119*, 5251−5252. (b) Bolton, K.; Hase, W. L.; Doubleday, C. *Ber. Bunsen-Ges. Phys. Chem.* **1997**, *101*, 414−422. (c) Doubleday, C.; Bolton, K.; Hase, W. L. *J. Phys. Chem. A* **1998**, *102*, 3648−3658.

(14) Hrovat, D. A.; Fang, S.; Borden, W. T.; Carpenter, B. K. *J. Am. Chem. Soc.* **1997**, *119*, 5253−5254.

(15) (a) Carpenter, B. K. *Acc. Chem. Res.* **1992**, *25*, 520. (b) Carpenter, B. K. *J. Am. Chem. Soc.* **1995**, *117*, 6336. (c) Carpenter, B. K. *J. Am. Chem. Soc.* **1996**, *118*, 10329. (d) Carpenter, B. K. *Angew. Chem., Int. Ed. Engl.* **1998**, *37*, 3341.

(16) Doering, W. v. E.; Sachdev, K. *J. Am. Chem. Soc.* **1974**, *96*, 1168.

(17) Baldwin, J. E. *J. Comput. Chem.* **1998**, *19*, 222−231.

(18) Doubleday, C.; Nendel, M.; Houk, K. N.; Thweatt, D.; Page, M. *J. Am. Chem. Soc.* **1999**, *121*, 4720.

(19) Dewar, M. J. S.; Hashmall, J. A.; Venier, C. G. *J. Am. Chem. Soc.* **1968**, *90*, 1953.

(20) Lewis, D. K.; Charney, D. J.; Kalra, B. L.; Plate, A.-M.; Woodard, M. H.; Cianciosi, S. J.; Baldwin, J. E. *J. Phys. Chem. A* **1997**, *101*, 4097.

(21) A very shallow minimum lies near (0, 180) at an energy 4.45 kcal/mol below TS13, with a structure that deviates from (0, 180) by a 5° conrotatory double rotation. The ZPE-corrected barrier to conrotatory cyclization is 0.1 kcal/mol.

(22) Bunker, D. L.; Hase, W. L. *J. Chem. Phys.* **1973**, *59*, 4621.

(23) Peslherbe, G. H.; Bolton, K.; Doubleday, C.; Hase, W. L. VENUS-MOPAC, a General Chemical Dynamics and Semiempirical Direct Dynamics Computer Program. To be released.

(24) Hase, W. L.; Duchovic, R. J.; Hu, X.; Komornicki, A.; Lim, K.; Lu, D. -h; Peslherbe, G. H.; Swamy, K. N.; Vande Linde, S. R.; Wang, H.; Wolfe, R. J.; VENUS 96, a General Chemical Dynamics Computer Program. *QCPE* **1996**, *16*, 671. VENUS 96 is an enhanced version of MERCURY: Hase, W. L.; *QCPE* **1983**, *3*, 453.

(25) (a) Stewart, J. J. P. MOPAC 7.0, a General Molecular Orbital Package, *QCPE* **1993**, 455. (b) Stewart, J. J. P. *J. Comput. Chem.* **1989**, *10*, 209.

(26) Doubleday, C.; Bolton, K.; Hase, W. L. *J. Phys. Chem. A* **1998**, *102*, 3648−58.

(27) Truhlar, D. G.; Muckerman, J. T. In *Atom-Molecule Collision Theory*; Berstein, R. B., Ed.; Plenum: New York, 1979; Chapter 16.

(28) Press: W. H.; Teukolsky, S. A.; Vetterling, W. T.; Flannery, B. P. *Numerical Recipes in Fortran; The Art of Scientific Computing*; University Press: Cambridge, 1992.

(29) Dewar, M. J. S.; Liotard, D. A. *J. Mol. Structure (THEOCHEM)* **1990**, *206*, 123.

(30) Pitzer, K. S.; Gwinn, W. D. *J. Chem. Phys.* **1942**, *10*, 428−440.

(31) Havlicek, L. L.; Crain, R. D. *Practical Statistics for the Physical Sciences*; American Chemical Society: Washington, DC, 1988; p 179.

(32) Table S7 of the Supporting Information gives information on trajectories that proceed through an anti biradical conformation. The product yields and ratios are grouped according to trajectories that do, and those that do not, proceed via an anti conformation.

(33) Constant angular velocity is rigorously expected only for free rotation of a symmetric group like methyl, for which the reduced moment of inertia does not depend on the torsion angle.

(34) (a) Peslherbe, G. H.; Hase, W. L. *J. Chem. Phys.* **1994**, *100*, 1179−89. (b) Guo, Y.; Thompson, D. L.; Sewell, T. D. *J. Chem. Phys.* **1996**, *104*, 576−582. (c) Lim, K. F. *J. Chem. Soc., Faraday Trans.* **1997**, *93*, 669−672. (d) Shen, D.; Chan, W.-T.; Pritchard, H. O. *Ibid.* **1995**, *91*, 3747.